

DESIGN AND SIMULATION OF THE CONTROLLED FAILURE OF CUSTOM-BUILT RIGID SHAFT COUPLING

Rasovic, N.*; Cekic, A.** & Kaljun, J.***

* University of Mostar, Faculty of Mechanical Engineering, Computing and Electrical Engineering, Matice Hrvatske bb, 88000 Mostar, Bosnia and Herzegovina

** University of Sarajevo, Faculty of Mechanical Engineering, Vilsonovo šetalište 9, 71000 Sarajevo, Bosnia and Herzegovina

*** University of Maribor, Faculty of Mechanical Engineering, Smetanova 17, 2000 Maribor, Slovenia
E-Mail: jasmin.kaljun@um.si

Abstract

In this paper, the use of conventional analytical calculating methods for designing the mechanical part with predicted endurance time is investigated. In a case study a design and dimensioning of custom-built shaft coupling with torque limiting function was conducted. Necessary analytical calculations were carried out to determine the possible weak points of the current shaft coupling design. Numerical analyses of the newly designed shaft coupling were performed using predefined material properties and boundary conditions. Using Goodman criteria, the most suitable design was selected. Prototypes of shaft couplings with different designs based on the numerical analysis were tested to validate the numerical results. Analytical approach as well as numerical analysis were compared. The validation of the produced machine part is also performed. Results of the research work showed that conventional analytical methods can be applied to design and dimension a mechanical part with predicted failure following steps (methodology) described in the paper.

(Received in November 2021, accepted in May 2022. This paper was with the authors 6 weeks for 1 revision.)

Key Words: Shaft Coupling, Design, Dimensioning, Fatigue, Simulation, Custom Design

1. INTRODUCTION

The shaft coupling plays a primary role in connecting two shafts in the process of torque transmission. Several types of these components are widely used in mechanical engineering, including rigid shaft couplings [1]. The shaft coupling, which is the subject of the presented research work, is a custom-designed machine element for connecting input and output shafts of two gearboxes (worm and spur gearboxes). The new rigid shaft coupling is installed as a replacement for the existing shaft coupling which does not have the function of torque limitation (Fig. 1).

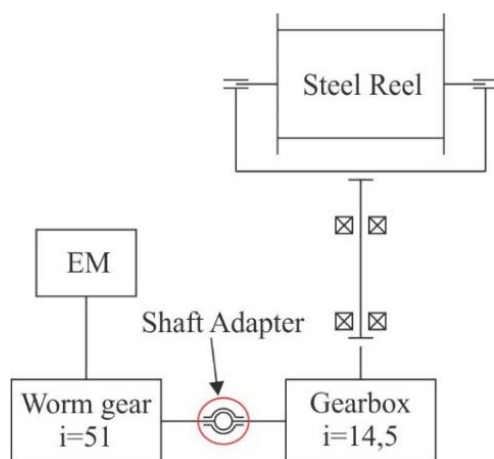


Figure 1: Schematic view of the workstation function.

Both gearboxes and their shaft coupling are part of the radial umbilical spooling machine of large diameters and high loads. For this reason, the entire construction is substantial and heavy, which presents a considerable challenge to normal functional performance. For safety reasons, it is necessary to investigate the possibility of developing a unique shaft coupling that also acts as a torque limiter in the function of preventing shaft and bearing damage. The analysis should also address the companies' demand to increase the load on the machine by 100 %. Preliminary calculations showed that the machine drive shaft would not be able to withstand the loads [2]. The fatigue analysis also showed that the drive shaft bearings could be damaged by the increase in shaft deformation.

Due to the shaft's predicted failure and bearing failure, an additional torque limiting system was considered, which could be implemented in the existing machine assembly. However, commercially available torque limiters were not suitable for the implementation because there was not enough space for the installation setup.

1.1 Research hypothesis

In general, mechanical design process is performed based on selected design/dimensioning approach, considering real or estimated boundary conditions. Design approaches are continuously developed in order to provide designers the most efficient method to dimension specific machine part.

Contrary to the usual use of dimensioning approach, where the designer wants to define a shape that will be able to permanently withstand the expected loads, presented research explored the possibility of applying the selected dimensioning approach in the case of defining the dimensions of machine part needed for controlled failure.

Analytical approach as well as numerical analysis were compared. After defining the shape, the validation of the produced machine part is also performed.

The goal of the research is to determine whether conventional analytical methods for calculating the endurance capacity are also useful for dimensioning a component with a known target number of loading cycles before failure.

1.2 Objective

In order to overcome the installation space limitations, it was decided to design and dimension a new shaft coupling with predicted failure in case of torque overload. In contrast to the usual research aimed at preventing failure [3-5], our primary goal is to cause failure under controlled and predicted conditions. The idea was supported by the fact that the replacement of the shaft coupling does not cause any significant difficulties.

To ensure a controlled coupling failure, the task will be carried out in the following steps: (1) analysis of the permanent strength of the existing coupling; (2) conception of the form of failure locations; (3) construction of a numerical model; (4) numerical calculation of fatigue; (5) verification of numerical results by physical tests; (6) defining the final shape of the coupling.

The redesigned shaft coupling must ensure stable operation under high load. In the event of a critical torque occurring, the shaft coupling must be broken. The main task is to obtain optimum design dimensions in order to ensure the failure of the shaft coupling instead of some other important components in case of excessive torque.

2. BOUNDARY CONDITIONS

The steel reel for the umbilical spooling of special wire ropes has a large diameter and the entire construction works under high loads. The total load value is 100 kN. For these reasons, the use

of spherical bearings is necessary. The calculation data to be used are: the input power of the electric motor is $P = 1.5 \text{ kW}$, the output shaft rate is $n = 2 \text{ min}^{-1}$.

The material selected for the shaft coupling is EN 1.4418, a high-strength martensitic/austenitic stainless steel with low carbon content [6]. The mechanical properties of the shaft coupling material are listed in Table I.

Table I: Mechanical properties of EN 1.4418.

Condition	Yield strength $RP_{0.2}$ [MPa]	Tensile strength R_m [MPa]	Elongation [%]
QT900	920	1050	18

In order to obtain data on the stress state data of the shaft coupling as a fuse, analytical and numerical calculations of the shear stress in characteristic cross-sections were carried out [7]. The matching of analytical and numerical calculations confirmed the suitability of the numerical model of the initial (existing) shaft coupling.

2.1 Initial design analysis

The currently used shaft coupling (Fig. 2) is a simple element with internal and external keyways used to connect the power and driven shaft. The basic geometrical properties of the initial shaft coupling are total length: 107 mm; diameter 1: 19 mm and diameter 2: 45 mm. A lateral keyway is provided on each diameter. The mass of the shaft coupling is 0.6 kg. A surface roughness value for all free surfaces on the part is $Ra = 3.2 \text{ mm}$, except for the specified surfaces where $Ra = 1.6 \text{ mm}$ applies.

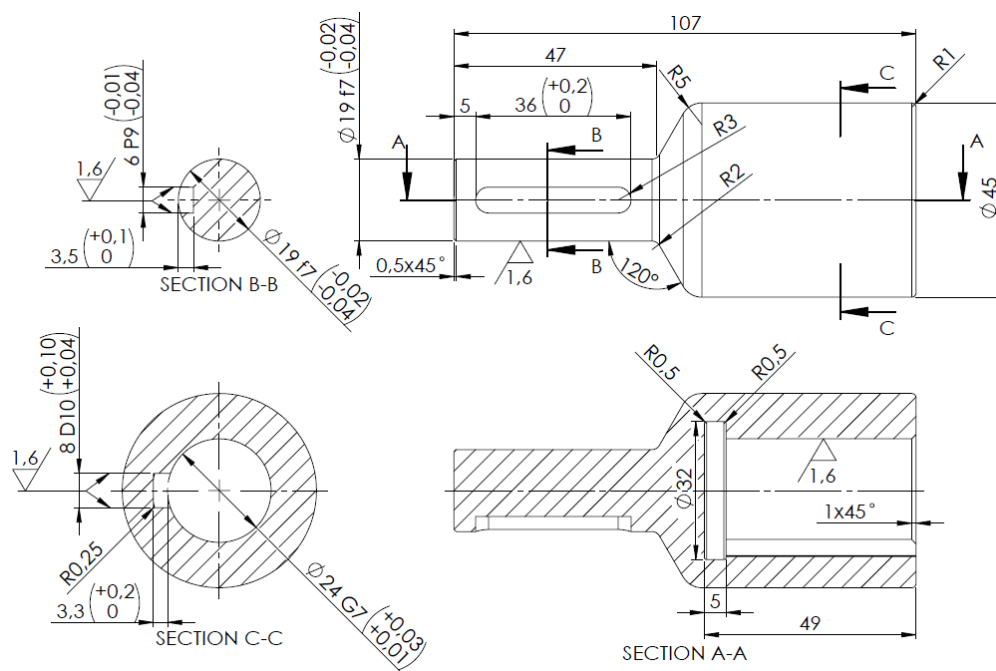


Figure 2: Detail drawing of the original shaft coupling.

3. ANALYTICAL CALCULATION OF THE SHAFT COUPLING

Analysis of the initial design offers 3 locations for predicted coupling failure (Fig. 3). Additional constraint implies that the failure location does not influence other vital assembly components in the sense of happening unexpected damage. Thus, the areas of the cross-sections

B-B and E-E are not desirable as failure position due to parallel key connection, as the most important representative type of shaft connection based on form fit. Given this fact, the cross-section D-D is the most suitable location to cause controlled failure due to following reasons:

- Predicted failure/fracture does not damage other assembly components,
- Due to geometric discontinuity, the geometric stress concentration factor influences stress amplification.

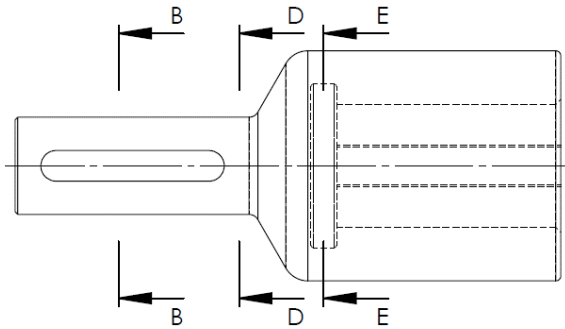


Figure 3: Observing the most important cross-sections.

As already mentioned in the Introduction, the torque overload case is rare but possible during the working process. Using the results of analytical calculation of shear stress and fatigue, the numerical model will eventually be validated.

The shear stress occurs in a cross-section as the most critical stress type for the shaft loaded by torque. Geometrical stability of the shape σ_o as dynamic endurance of a specific shaft cross-section must be smaller than the product of dynamic variable endurance of material and factor of stability of the shape. The geometrical stability of the shape σ_o , as dynamic endurance of a specific shaft cross-section, is defined by Eq. (1a). The discontinuity of geometry has a significant effect on the stress distribution around it. Geometric stress concentration factors are used to estimate the stress amplification in the vicinity of a geometric discontinuity. Accordingly, Eq. (1b) presents a stress concentration factor of a circular shaft [8].

$$\sigma_o = \frac{\sigma_{DN} \cdot k_s}{K_{ts} \left(1 - \frac{\sigma_{sr}}{\sigma_g}\right)} \leq k \cdot \sigma_{DN} \quad \text{a)}$$

$$K_{ts} = 1 + \frac{1}{\sqrt{\frac{\varepsilon_1}{\frac{c}{\rho}} + \frac{\varepsilon_2 \left(1 + \frac{d}{2\rho}\right)^2}{\left(\frac{d}{2\rho}\right)^3} + \frac{\varepsilon_3}{\left(\frac{c}{\rho}\right)^3}}} \quad \text{b)}$$

In the case of the torsional loaded shaft, it is recommended that the minimum required shaft diameter must be defined according to experiential values of allowable using Eq. (2a).

$$d_{min} = \sqrt[3]{\frac{T}{0.2\tau_{allow.}}} \quad \text{a)}$$

$$\tau_{t_nom} = \frac{T}{W_t} \leq \tau_{allow.} \quad \text{b)}$$

$$\tau_{t_max} = K_{ts} \frac{T}{W_t} \leq \tau_{allow.} \quad \text{c)}$$


The maximum and the minimum shear stress occurring at the critical cross-section of the shaft are considered. Only the weight of an empty steel reel and its inertial masses produce minimum stress. It takes the torque of $T = 200$ Nm to drive all rotating components in the idle.

Using the output shaft rate at steel reel, the transmission ratio of the gearbox, fully loaded steel reel and its inertial masses, maximum calculated torque to the entrance of gearbox is

$T = 504$ Nm. Nominal shear stress is calculated using Eq. (2b) based on calculated torque and torsional section modulus.

Table II shows analytical calculations of torsional section modulus and stress values, nominal, minimal and maximum. Using the expression shown by Eq. (2c) and its influence on the stress amplification-based to the shaft geometry, the maximum torsional stress is 598.76 MPa. Minimal torsional stress is calculated respectively, using minimal (idle) torque. Both stress values (τ_{t_nom} , τ_{t_max}) satisfy the limit of allowable shear strength.

Table II: Torsional section modulus and shear stress values for the D-D cross-section.

	Shape	d [mm]	ε_1	ε_2	ε_3	K_{ts}	$W_{t\ D-D}$ [mm ³]	τ_{t_nom} [MPa]	τ_{t_min} [MPa]	τ_{t_max} [MPa]
Section D-D		19	3.4	6	0.2	1.6	1346.76	374.23	237.6	598.76

3.1 Fatigue analysis

For dynamically loaded shaft coupling, the failure occurs at lower stress than the allowable stress is. Fatigue tests for notched or un-notched specimens are necessary to calculate fatigue life in the case of realizing controlled failure [9]. For a qualitative estimate, we made a comparison between analytical and numerical fatigue solutions. Previously conducted data represents a base for fatigue tests. Fatigue strength depends on not only the stress concentration factor but also other factors such as the material strength, mean and amplitude stress levels. As a base for estimating the effect of all parameters, it is used zero-based loading type and long life of $N = 10^8$ cycles to failure. Using Goodman's theory [10-13] fatigue factor of safety $EFoS$ is calculated according to Eq. (3a) considering the fatigue stress concentration factor K_{fts} , Eq. (3b), the notch sensitivity q , Eq. (3c), of the material and its tensile strength.

$$\frac{1}{EFoS} = \frac{S_m}{R_m} + \frac{S_a \cdot K_{fts}}{S'_e \cdot k_s \cdot k_d} \quad K_{fts} = 1 + q(K_{ts} - 1) \quad q = (1.4 \dots 0.8)10^{-3}R_m \leq 1 \quad (3)$$

a) b) c)

The fatigue ranges from 40 to 60 % of the tensile strength for the steels up to 1400 MPa of tensile strength [14, 15]. If we take the upper range limit, endurance limit S_e of the shaft coupling material is calculated using Eq. (4a). Various correction factors influence the fatigue strength. Correction factors: reliability factor (for 90 % reliability) $k_R = 0.897$ and surface factor (fine polished) $k_s = 0.95$ are selected; size factor k_d is calculated using Eq. (4b). Using Eq. (4c) correction factors, the new fatigue strength S'_e is calculated. Finally, for torsional loading, the fatigue strength at 1000 cycles ($k_R = 0.897$ for 90 % reliability) is calculated using Eq. (4d) [14].

$$S_e = 0.6 R_m \quad k_d = (d/7.62)^{-0.107} \quad S'_e = S_e \cdot k_s \cdot k_d \cdot k_R \quad S_{e1000} = 0.9(0.8R_m)k_R \quad (4)$$

a) b) c) d)

To determine fatigue or endurance factor of safety ($EFoS$), we calculated mean stress (S_m) and amplitude stress (S_a) based on maximum (S_{max}) and minimum (S_{min}) stress values. Maximum stress value occurs at the fully loaded mode, while minimum stress occurs at the idle. We start from the assumption that failure always occurs at the critical zone at maximum stress value caused during extreme loading conditions. Therefore, variable amplitude stress is being transformed into constant amplitude stress to calculate mean stress. Using the highest torque value required to drive a fully loaded machine, maximum stress is: $S_{max} = 598.76$ MPa. The same as previous, using the minimum required torque value to drive the machine in the

idle, minimum stress is: $S_{min} = 237.6$ MPa. Mean stress value and amplitude stress value are presented in Table III.

Table III: Analytical solution results of mean and amplitude stress including fatigue factor of safety.

	S_m [MPa]	S_a [MPa]	q	K_{fts}	$EFoS$
Original configuration	418	180	0.84	1.5	1.05

Analytically calculated fatigue safety factor ($EFoS$) expresses low confidence and reliability of endurance in the case of extreme loading conditions. For a thorough analysis of the fatigue life, the cycle is estimated by the following assumption: the steel reel rotates at a speed of 2 rpm. In eight working hours, it rotates 960 times, then in one year for 360 working days, it rotates 345600 times, and in five years (predicted life of the workstation), it rotates 1728000 times. The predicted life of the shaft coupling is obtained by multiplication of the last number with a transmission ratio of 14.5. Considering these explanations, the predicted life of the shaft coupling is approximately $N = 2.5 \text{ E}+07$. The endurance limit is determined on the basis of the high cycle region of $N_f = 1.0 \text{ E}+08$ cycles to failure.

To create an $S-N$ curve using predicted shaft coupling lifetime and endurance limit, the following Eq. (5) is used:

$$S_{N(N)} = S'_e \left(\frac{N_f}{N} \right)^{\frac{1}{m}}; m = 10 \tag{5}$$

Fig. 4 shows the Wohler's $S-N$ curve for the original configuration based on the endurance limit of $N_f = 1.0 \text{ E}+08$ load cycles to failure. To get more data points in creating a smooth curve, a various number of cycles was included in Eq. (5), starting from $5.0 \text{ E}+05$ cycles, as the low cycle region. All data points are logarithmically presented along the horizontal axis, while the vertical axis shows stress values.

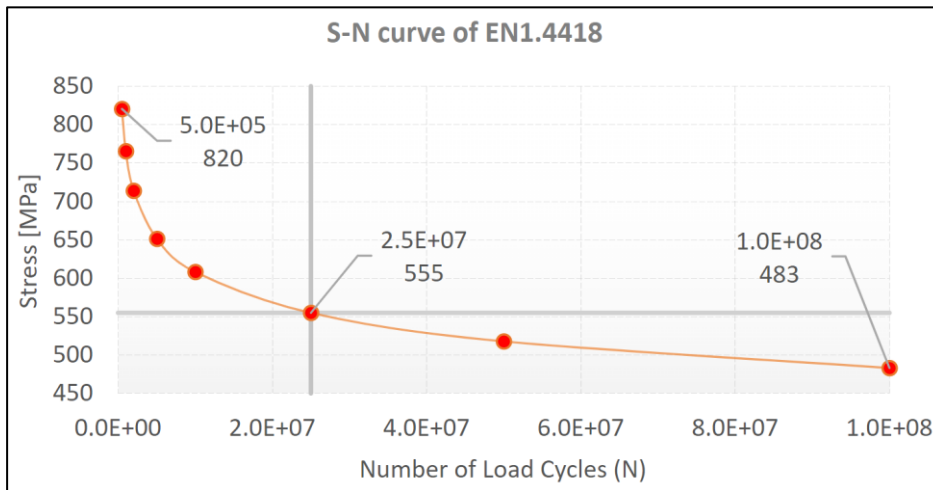


Figure 4: Wohler's $S-N$ curve; Low cycle region, $N = 5.0 \text{ E}+05$; High cycle region, $N_f = 1.0 \text{ E}+08$.

Using Eq. (5) in combination with the characteristic number of load cycles, the Wohler's $S-N$ curve was created, bounded between two intervals, low cycle region and high cycle region. The stress value obtained using Eq. (5) presents ultimate (short-lived) dynamic strength for a characteristic number of load cycles. Observing $S-N$ curve, the ultimate (short-lived) stress value for the predicted lifetime at $N = 2.5 \text{ E}+07$ cycles is 555 MPa. Compared with the maximum stress (555.56 MPa) calculated by numerical solution (discussed in continuation), the relation satisfies the ultimate strength condition. The maximum stress (598.76 MPa)

calculated by the analytical solution exceeds the ultimate strength limit. Nevertheless, as we already said, it is the more conservative result at the upper range limit so that we can interpret it as acceptable.

By Goodman's theory and calculated fatigue factor of safety, it has also been determined ultimate stress value for the predicted life. According to that, the original shaft coupling design will endure the outlined number of load cycles and more.

4. NUMERICAL ANALYSIS OF THE SHAFT COUPLING

4.1 Static structural analysis

In the further research process, the analytical solution is used to verify the numerical model using finite element analysis for additional accuracy and validation of the results. Fig. 5 shows the parameterized FE model with defined mesh parameters.

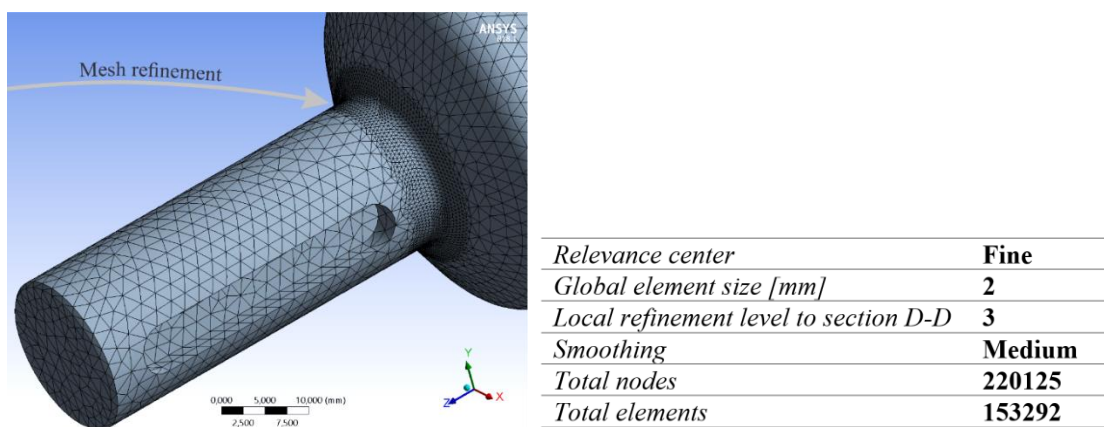


Figure 5: Parameterized FE model with defined mesh parameters with parameters.

The data represent a continuum discretized by finite elements, with three degrees of freedom in each node. Discretization may be described as a process by which the given body is subdivided into an equivalent system of finite elements.

Static structural analysis as a part of FEA is conducted in the Ansys Workbench (Fig. 6). The geometry used to calculate shear stress is shown in Fig. 3. Using two different torques required driving the idle and fully loaded mode, numerical solution verifies stress calculation done before in analytical procedure. The criterion for a decision whether the construction is in failure condition was: if the shear stress is greater than the allowable stress of the material, then the construction is in failure condition. The material used in FEA for the shaft coupling belongs to Ansys Workbench Materials, and it is equivalent to EN 1.4418.

According to the applied torques, boundary conditions of the parameterized model and material properties, shear stress results are expressed (Fig. 6). Maximum shear stress in the fully loaded mode is 555.56 MPa respect to the analytical solution of 598.76 MPa (Table II) in the critical zone D-D. The slight difference between the two kinds of results is addressed to the more conservative method we used in the definition of the stress concentration factor. The difference is also reflected in the opposite direction of calculation in the idle. Minimum shear stress in the idle is 220.46 MPa respect to the analytical solution of 237.6 MPa. Analytical solution results are expected to be higher due to the geometric stress concentration factor. The geometric curvature of the long slope between two shaft diameters has greatly influenced the high value of the stress concentration factor (K_{ts}). Using this verification step, stress results of both calculation solutions have been verified. Now, we have determined stress around the critical area of the cross-section D-D using static structural analysis.

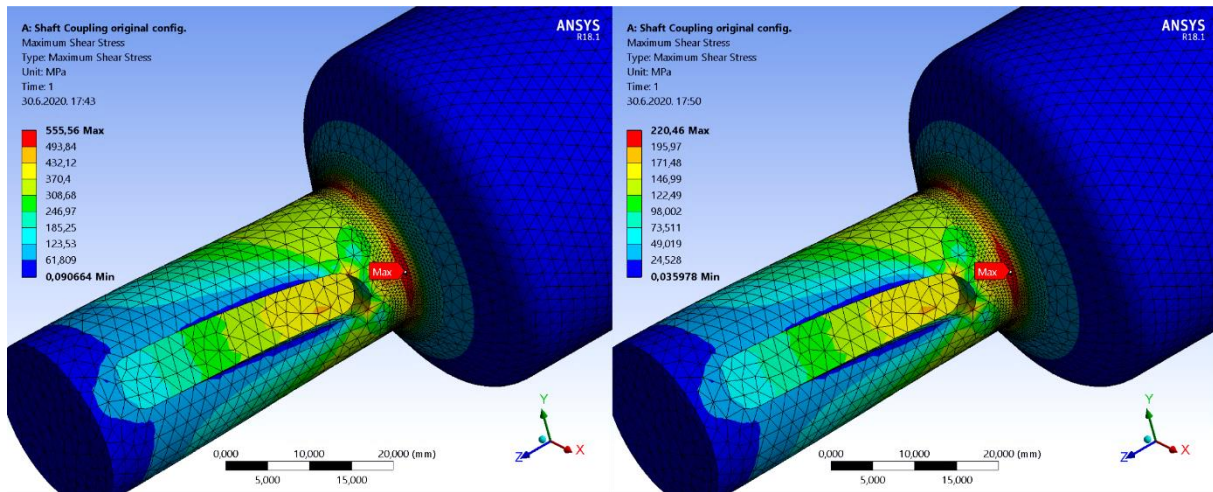


Figure 6: Results of static structural analysis: maximum shear stress in the fully loaded mode ($\tau_{t,max}$) and the idle ($\tau_{t,min}$).

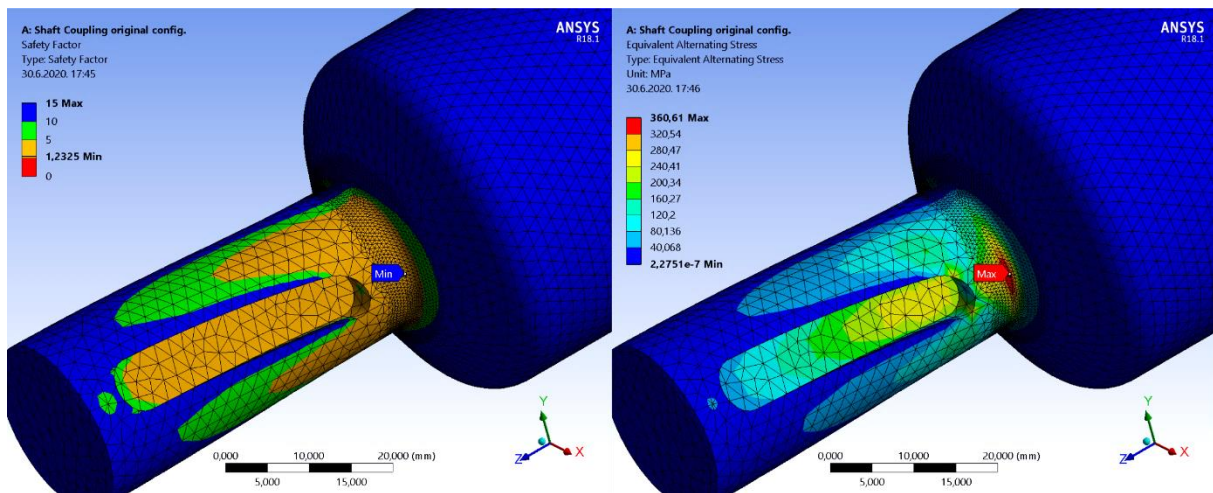


Figure 7: Calculated *EFoS* and equivalent alternating stress for the case of constant amplitude loading.

Previous conducted analytical solution of the fatigue analysis and its numerical solution are being compared. Using the same mesh parameters as in previous analyses, the numerical solution shows the fatigue safety factor of 1.2325 for the critical zone (Fig. 7). Using the endurance limit of $N_f = 1.0 \text{ E}+08$ cycles to failure the result indicates the infinite life for the set parameters. Since the fatigue safety factor calculated by the numerical solution is greater than the analytical, the relation between safety factors also confirms the conservative approach we have chosen for the analytical solution. For a further fatigue analysis, the equivalent alternating stress is additionally used to query the *S-N* curve with a defined loading type. Since loading has a constant maximum value during extreme conditions, only one set of FE stress results is required to calculate alternating stress, which makes loading proportional (stress does not change over time).

Regarding constant amplitude loading and respect to the zero-based measuring, it can be identified as critical fatigue locations. Therefore, we introduce the equivalent alternating stress as the last calculated stress amount before determining fatigue. Based on conducted fatigue analysis (Fig. 7), the equivalent alternating stress is 360.61 MPa. Since the alternating stress we consider as the last calculated value, it is acceptable not only for the predicted life ($N = 2.5 \text{ E}+07$) but also for the high cycle region ($N_f = 1.0 \text{ E}+08$). According to the comprehensive analysis, the original shaft coupling has to be redesigned.

5. REDESIGN FOR CONTROLLED FAILURE

To achieve the required task of the shaft coupling, the intention is to add a groove in the cross-section D-D [16]. Redesign configuration must ensure enough amount of stress concentration to cause controlled failure in acceptable timeframe under overload. According to that, the decision has been made to design and dimension two types of grooves: rectangular and trapezoidal at the location of the maximum shear stress (Fig. 8). Semi-circular groove is not considered due to its favourable influence of shape geometry to stress concentration decreasing.

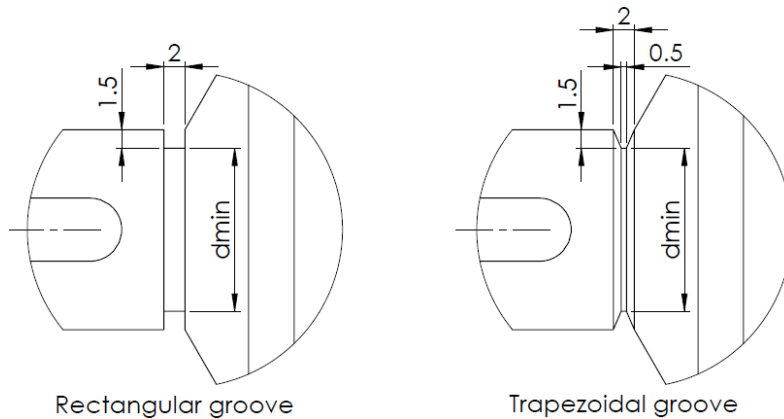


Figure 8: Rectangular and trapezoidal grooves with detailed dimensions.

Taking into account groove machining technology, to create appropriate grooves shown in Fig. 8, the smallest cutting tool dimensions are used. Groove width of 2 mm is a tool entrance while cutting depth is defined by the expression in Eq. (2a) and is equal to 1.5 mm. Grooves are modelled in rectangular and trapezoidal forms (Fig. 8). Using the same boundary conditions (mesh settings and parameterized model) as it was presented in previous conducted FE analysis, a new fatigue analysis of redesign configurations has been carried out.

Fig. 9 shows the graphic representation of stress distribution. The shaft coupling configuration including rectangular groove ensures $N = 236$ cycles against $N = 34$ cycles for the trapezoidal groove configuration. The cycles' relation between these two redesign configurations was expected (the configuration with a trapezoidal groove is more unfavourable), but the exact number of cycles to failure has not been known before.

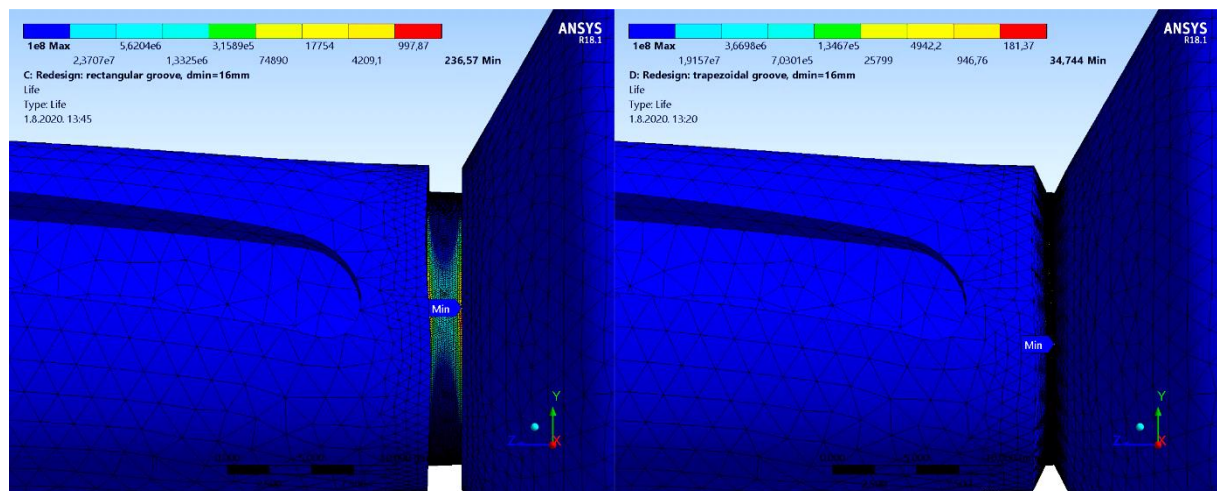


Figure 9: Estimated life of the redesign configurations with rectangular and trapezoidal grooves for $d_{min} = 16$ mm.

6. EXPERIMENTAL VALIDATION AND RESULTS DISCUSSION

To validate the numerical simulation and define the number of cycles to failure under overload, we performed experimental testing of prepared specimens. Zwick dynamic testing machine was adapted to conduct dynamic measurements with a determined number of repeats necessary to simulate cycles to failure. To simulate torque transmission over specimen body, torque wrench was installed on the testing machine. The used torque wrench has a capacity range between 400-800 Nm. In the case of our testing, it is calibrated to 504 Nm, which value was calculated before [2]. The used testing technique has disparities of ± 50 Nm in achieving maximum torque, which is seen by the height of the peaks (Fig. 10).

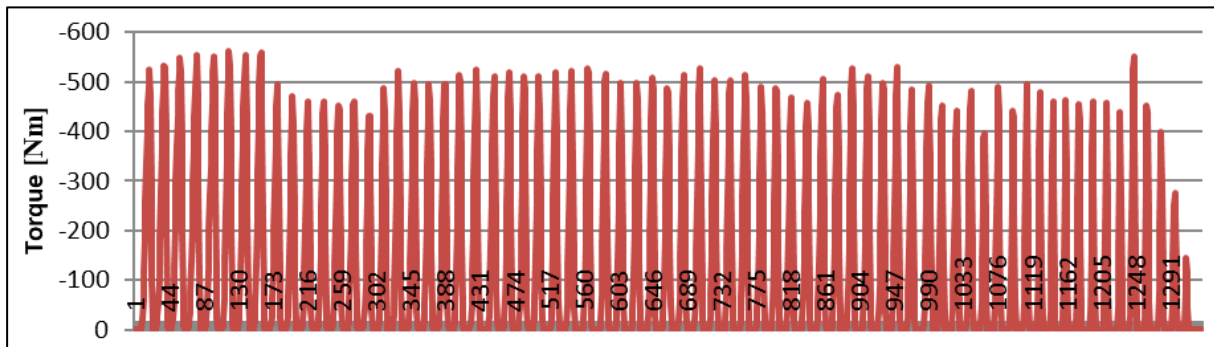
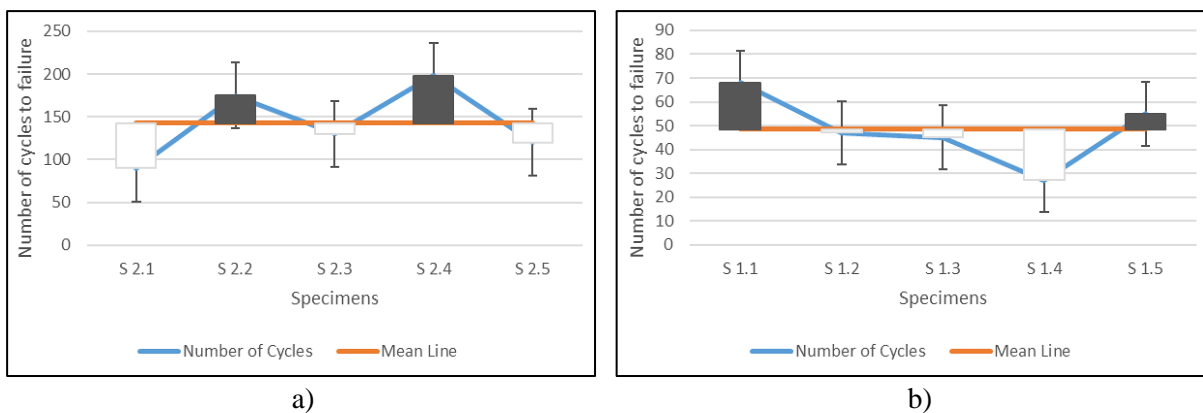


Figure 10: Experimental life measuring of configuration with trapezoidal groove, $d_{min} = 16$ mm.

Contributing to the better results reliability, we conducted experimental testing using five specimens for each groove shape. For further analysis, we only used the four results that were closest to the mean value.

As predicted, specimens with rectangular grooves withstand a much greater number of cycles before failure and therefore longer life under extreme loading conditions. Comparing to numerical results, a larger difference is noticed in the case of rectangular grooves. The difference between the highest and the smallest number of cycles to failure is 78. The mean value represented by a mean line on a diagram (Fig. 11 a) is 155.75, and the standard deviation is 32.00 (covering 60 % of all results obtained by experimental testing). Upper boundary value as the ultimate limit of results reliability ($\bar{x} + \sigma = 187.75$) does not match with the numerical solution of 236.57 cycles to failure. The difference can be assigned to the imperfection of the machining (cutting operations), which is reflected in the specimens.



rectangular groove: $n_s = 5$; $\bar{x} = 142.6$; $\sigma_{st} = 38.87$

trapezoidal groove: $n_s = 5$; $\bar{x} = 48.4$; $\sigma_{st} = 13.41$

Figure 11: Standard deviation for specimens.

In the case of specimens with trapezoidal groove shape, the results are closer to each other that is visible from a diagram scale in Fig. 11 b. Experiments have shown that specimens with this type of groove withstand fewer loading cycles and therefore, shorter life under extreme loading conditions. The results have not been scattered and the difference between the highest and the smallest number of cycles to failure is 21. The mean value represented by a mean line on a diagram (Fig. 11 b) is 53.75 and standard deviation of 9.04 (60 % of all results obtained by experimental testing). Lower boundary value as the ultimate limit of results reliability ($\bar{x} - \sigma = 44.71$) almost matches with the numerical solution of 34.74 cycles to failure. This fact confirms the high reliability of results as well as their consistency in obtaining a reliable number of cycles to failure. Again, the difference can be assigned to the imperfection of the machining (cutting operations), which is reflected in the specimens.

Results obtained by experimental dynamic testing ensure a certain number of cycles to failure under extreme loading conditions. In dynamic types of tests, it is difficult to expect a large number of matches at measured results values. However, less scattering of results is expected as an indicator of better reliability and consistency.

Using applied analysis and appropriate solution, redesigned configurations will endure between 5.3 minutes (for specimens with rectangular groove) and 1.6 minutes (for specimens with trapezoidal groove) to failure under extreme loading conditions.

7. CONCLUSION

This paper presents the results of the analytical, numerical and experimental study on the controlled failure of the shaft coupling. Although it is a matter of solving a specific problem from the industry, a methodology has been set up. Shear stress caused by the maximum torque was determined and located. On that basis, fatigue strength and the number of cycles to failure are determined considering the factor of safety as high enough. According to that, the presented study aims to design and dimension the controlled weak position on the shaft coupling. To prevent bearings and shafts damage, redesign of the shaft coupling was made in the direction of achieving controlled weak position. Minimum diameter and dimensions for making grooves are defined. By this way, the minimum number of cycles to failure was ensured.

Results of the studies conducted show that conventional analytical methods for calculating the endurance capacity can be used for dimensioning a component with a known target number of loading cycles before failure. The paper's main contribution is based on the presented methodology of design and dimensioning the controlled failure of custom-built rigid shaft coupling, which has been thoroughly developed and described.

REFERENCES

- [1] Lee, H. W.; Han, J. Y.; Kang, J. H. (2016). A study on high speed coupling design for wind turbine using a finite element analysis, *Journal of Mechanical Science and Technology*, Vol. 30, No. 8, 3713-3718, doi:[10.1007/S12206-016-0733-1](https://doi.org/10.1007/S12206-016-0733-1)
- [2] Rašović, N.; Vučina, A.; Dedić, R. (2019). Design and analysis of steel reel shaft by using FEA, *Technical Gazette*, Vol. 26, No. 2, 527-532, doi:[10.17559/TV-20180116103950](https://doi.org/10.17559/TV-20180116103950)
- [3] Savković, M.; Gašić, M.; Petrović, D.; Zdravković, N.; Pljakić, R. (2012). Analysis of the drive shaft fracture of the bucket wheel excavator, *Engineering Failure Analysis*, Vol. 20, 105-117, doi:[10.1016/j.engfailanal.2011.11.004](https://doi.org/10.1016/j.engfailanal.2011.11.004)
- [4] Liu, Y.; Lian, Z.; Xia, C.; Qian, L.; Liu, S. (2019). Fracture failure analysis and research on drive shaft of positive displacement motor, *Engineering Failure Analysis*, Vol. 106, Paper 104145, 18 pages, doi:[10.1016/j.engfailanal.2019.08.011](https://doi.org/10.1016/j.engfailanal.2019.08.011)
- [5] Szávai, S.; Kovács, S.; Bézi, Z.; Kozak, D. (2021). Coupled numerical method for rolling contact fatigue analysis, *Technical Gazette*, Vol. 28, No. 5, 1560-1567, doi:[10.17559/TV-20201117124940](https://doi.org/10.17559/TV-20201117124940)

- [6] Monnot, M.; Nogueira, R. P.; Roche, V.; Berthomé, G.; Chauveau, E.; Estevez, R.; Mantel, M. (2017). Sulfide stress corrosion study of a super martensitic stainless steel in H₂S sour environments: Metallic sulfides formation and hydrogen embrittlement, *Applied Surface Science*, Vol. 394, 132-141, doi:[10.1016/j.apsusc.2016.10.072](https://doi.org/10.1016/j.apsusc.2016.10.072)
- [7] Kalayci, C. B.; Karagöz, S.; Karakaş, Ö. (2019). Bee colony intelligence in fatigue life estimation of simulated magnesium alloy welds, *International Journal of Fatigue*, Vol. 127, 36-44, doi:[10.1016/j.ijfatigue.2019.05.032](https://doi.org/10.1016/j.ijfatigue.2019.05.032)
- [8] Vitas, D. J. (1989). *Osnovi mašinskih konstrukcija* (7th ed.), Naučna knjiga, Beograd (in Serbian)
- [9] Wang, Z.; Li, B.; Liang, C.; Wang, X.; Li, J. (2021). Response analysis of a scraper conveyor under chain faults based on MBD-DEM-FEM, *Strojniski vestnik – Journal of Mechanical Engineering*, Vol. 67, No. 10, 501-515, doi:[10.5545/SV-JME.2021.7300](https://doi.org/10.5545/SV-JME.2021.7300)
- [10] Hasap, A.; Paitekul, P.; Noraphaiphaksa, N.; Kanchanomai, C. (2018). Analysis of the fatigue performance of elastic rail clip, *Engineering Failure Analysis*, Vol. 92, 195-204, doi:[10.1016/j.engfailanal.2018.05.013](https://doi.org/10.1016/j.engfailanal.2018.05.013)
- [11] Pallarés-Santasmartas, L.; Albizuri, J.; Avilés, A.; Saintier, N.; Merzeau, J. (2018). Influence of mean shear stress on the torsional fatigue behaviour of 34CrNiMo6 steel, *International Journal of Fatigue*, Vol. 113, 54-68, doi:[10.1016/j.ijfatigue.2018.04.008](https://doi.org/10.1016/j.ijfatigue.2018.04.008)
- [12] Glamsch, J.; Deese, K.; Rieg, F. (2019). Methods for increased efficiency of FEM-based topology optimization, *International Journal of Simulation Modelling*, Vol. 18, No. 3, 453-463, doi:[10.2507/IJSIMM18\(3\)482](https://doi.org/10.2507/IJSIMM18(3)482)
- [13] Yang, L.; Yang, B.; Yang, G. W.; Xiao, S. N.; Zhu, T.; Wang, F. (2020). S-N curve and quantitative relationship of single-spot and multi-spot weldings, *International Journal of Simulation Modelling*, Vol. 19, No. 3, 482-493, doi:[10.2507/IJSIMM19-3-CO11](https://doi.org/10.2507/IJSIMM19-3-CO11)
- [14] Lee, Y.-L.; Taylor, D. (2005). 4 - Stress-Based Fatigue Analysis and Design, Lee, Y.-L.; Pan, J.; Hathaway, R. B.; Barkey, M. E. (Eds.), *Fatigue Testing and Analysis (Theory and Practice)*, Butterworth-Heinemann, Burlington, 103-180, doi:[10.1016/B978-075067719-6/50005-1](https://doi.org/10.1016/B978-075067719-6/50005-1)
- [15] Cianetti, F. (2020). How to experimentally monitor the fatigue behaviour of vibrating mechanical systems?, *Strojniski vestnik – Journal of Mechanical Engineering*, Vol. 66, No. 10, 557-566, doi:[10.5545/SV-JME.2020.6853](https://doi.org/10.5545/SV-JME.2020.6853)
- [16] Ahsan, R. U.; Prachurja, P.; Ali, A. R. M.; Mamun, M. A. H. (2013). Determination of effect of elliptic notches and grooves on stress concentration factors on notched bar in tension and grooved shaft under torsion, *Journal of Naval Architecture and Marine Engineering*, Vol. 10, No. 1, 25-32, doi:[10.3329/jname.v10i1.13675](https://doi.org/10.3329/jname.v10i1.13675)